Available online at www.sciencedirect.com
SCIENCE DIRECT®
International Journal of Heat and Mass Transfer 49 (2006) 4536–4542
International Journal of HEAT and MASS TRANSFER
www.elsevier.com/locate/ijhmt

Application of multiple magnetic coils to drive the air flow in a long pipe

Shu-Shen Lu [a,*], Hiroyuki Ozoe [b]

[a] School of Chemistry and Chemical Engineering, Sun Yat-Sen University, Guangzhou 510275, China
[b] Formerly Kyushu University, Kasuga, Japan

Received 5 September 2005; received in revised form 5 March 2006
Available online 10 July 2006

Abstract

The laminar air flow in a pipe is studied with application of multiple magnetic fields at the point of uniform heat flux heating from the wall as the first boundary conditions. As the second boundary condition, after a coil, uniform heat flux heating and then uniform heat flux cooling from the wall is applied. Numerical computations are successfully carried out by solving transient 2-D equations with pressure gradient boundary condition for three lengths of pipe and two boundary conditions. The first one is for a ratio of pipe length and diameter $L = 10$ with a single electric coil. The second one is for $L = 20$ with two electric coils and the third one is for $L = 30$ with three electric coils to generate the magnetic field. A parameter ξ is from 0 to 2×10^7, which represents the strength of the magnetic field and the uniform heat flux from the pipe wall. The results show that the volume flow rate increases with the strength of magnetic field. Magnetic fields generated by the multi-coils can drive the air flow in the corresponding longer pipe almost equally to the shorter one with a single coil. From the distributions of the cross-sectional magnetic force along the pipe length, the effect of pressure, pressure gradient distribution along the pipe length, and the effect of gradient magnetic field and temperature field on the overall air flow rate can be analyzed and compared on the effect of wall cooling.

Keywords: Magneto-thermal convection; Magnetic force; Numerical heat transfer; Static boundary condition

1. Introduction

Uetake et al. [1,2] firstly reported the enhanced air flow rate in a pipe partly heated from a tube wall with an application of a strong magnetic field and they named this as a magneto-thermal wind tunnel. They placed the heated part at the off-center of the solenoid coil of magnet. Since air contains oxygen whose mass magnetic susceptibility is exceptionally large (paramagnetic fluid), heated air is repelled from the strong magnetic field while the non heated colder air is attracted from the solenoid center. The bulk air is driven as the difference between these two forces in the pipe toward the heated air area. Lu et al. [3,4] computationally studied this problem both with constant wall temperature and uniform heat flux at a latter half of a tube with an application of a magnetic coil at the center of a pipe, and found not only the enhancement of flow rate, but the enhanced rate of heat transfer compared with the classical Graetz solution. This magneto-thermal wind tunnel for paramagnetic fluid has a number of privileges such as no moving parts and no electricity required and particularly suitable for the application for space station.

Depending on the value of magnetic susceptibility, the weak magnetic materials can be classified into paramagnetic one (with positive value such as oxygen gas, $\chi_{m0} = 1.91 \times 10^{-6}$) and diamagnetic one (with negative value such as water, $\chi_{m0} = -9.02 \times 10^{-6}$). The paramagnetic materials are attracted to the magnetic field, while the diamagnetic ones are repelled from the magnet field. This magnetic force is expressed as follows according to Bai et al. [5]:

$$\vec{f}_m \cong \frac{\chi_{m0}}{2\mu_m}\vec{\nabla}b^2 = \frac{\rho_0\chi_0}{2\mu_m}\vec{\nabla}b^2 \quad (1)$$

* Corresponding author. Tel.: +86 20 84112151; fax: +86 20 84112150.
E-mail address: lvshsh@mail.sysu.edu.cn (S.-S. Lu).

0017-9310/$ - see front matter © 2006 Elsevier Ltd. All rights reserved.
doi:10.1016/j.ijheatmasstransfer.2006.04.034

Nomenclature

A	cross-sectional area $= (\pi d^2)/4$ [m^2]
B	magnetic induction [$T = Wb/m^2 = kg\ s^{-2}\ A^{-1}$]
b_0	$\mu_m i/d$ [$T = Wb/m^2 = kg\ s^{-2}\ A^{-1}$]
B	dimensionless magnetic induction vector $= b/b_0$ [–]
C_{p0}	specific heat of air [J/kg K]
d	diameter of a pipe [m]
f_m	magnetic force [N]
F_{mz}	Z-directional magnetic force integrated in each cross-section $= 8 \cdot \int_0^{0.5} [-\xi \Theta (\partial B^2/\partial Z)] R\, dR$
Gr^*	modified Grashof number $= g\beta_0 d^3 T_{ref}/\nu_0^2$ [–]
i	electric current in a coil [A]
j	the jth of electric coils [–]
l	length of a pipe [m]
L	dimensionless length of pipe $= l/d$ [–]
n	number of electric coils [–]
p	pressure [Pa]
P	dimensionless pressure $= p/(\rho_0 \nu_0^2/d^2)$ [–]
Pe	Peclet number $= Re \cdot Pr$ [–]
Pr	Prandtl number $= \nu_0/\alpha_0$ [–]
q_w	wall heat flux [J/m^2 s]
Q	volume flow rate $= A w_a$ [m^3/s]
r	radial coordinate. For the electric coil system, distance from coil segment to a point inside the pipe [m]
R	r/d. For the electric coil system, dimensionless distance from coil segment to a point inside the pipe [–]
Re	Reynolds number $= (w_a d)/\nu_0 = 4Q/(\pi \nu_0 d)$ [–]
Re_0	Reynolds number without a magnetic field [–]
s	a segment of the coil [m]
S	dimensionless length of the coil $= s/d$ [–]
t	time [s]
T	temperature [K]
T_a	mixing temperature at $z = \left(\int_0^{d/2} 2\pi r \cdot w \cdot T\, dr\right) \Big/ \left(\int_0^{d/2} 2\pi r \cdot w\, dr\right)$ [K]
T_i	inlet air temperature [K]
T_{ref}	$(-q_w d)/\lambda_0$ for heating and $(q_w d)/\lambda_0$ for cooling [K]
T_w	wall temperature [K]
u	velocity component in the radial direction [m/s]
U	$u/(\nu_0/d)$ [–]
w	velocity component in the axial direction [m/s]
w_a	average velocity in the axial direction $= \left(\int_0^{d/2} 2\pi r w\, dr\right) \Big/ \left(\int_0^{d/2} 2\pi r\, dr\right)$ [m/s]
W	$w/(\nu_0/d)$ [–]
z	axial coordinate [m]
Z	z/d [–]

Greek symbols

α_0	thermal diffusivity of air $= \lambda_0/(\rho_0 C_{p0})$ [m^2/s]
β_0	volumetric coefficient of expansion [1/K]
γ	$\chi_{m0} b_0^2/(g\mu_m d)$ [–]
Θ	dimensionless temperature $= (T - T_{in})/T_{ref}$ [–]
λ_0	thermal conductivity of air [W/m K]
μ_m	magnetic permeability [H/m]
ν_0	kinematic viscosity of air [m^2/s]
ξ	dimensionless value representing the strength of magnetic field, temperature difference and diameter of the pipe $= \gamma \cdot Gr^* = \frac{\chi_{m0} b_0^2}{g\mu_m d} \cdot \frac{g\beta_0 d^3 T_{ref}}{\nu_0^2}$ [–]
ρ_0	density of air [kg/m^3]
τ	dimensionless time $= t/(d^2/\nu_0)$ [–]
χ_0	mass magnetic susceptibility of air [m^3/kg]
χ_{m0}	volume magnetic susceptibility of air [–]

Subscripts

0	reference, or without magnetic field
a	average
c	axial line of the pipe
in	inlet
m	magnetic
max	maximum
ou	outlet
w	wall
z	local value along the axial coordinate

According to the Curie's law, the mass magnetic susceptibility χ_0 of a paramagnetic material is inversely proportional to its absolute temperature. Thus a paramagnetic fluid receives different forces from the gradient magnetic field depending on the temperature inside the fluid and convection is resulted. For the practical application of this phenomenon it may be necessary to treat the long pipe. For a long pipe single coil driving may not be enough and herein we try to consider multiple coils. In the present report, multiple coils or magnets are proposed to compare the effects of numbers of magnetic coil, pipe length and strength of magnetic field.

2. Model system

The pipe considered has a diameter d and length l, with multiple electric coils whose diameter is twice of the pipe to generate magnetic fields. Fig. 1 shows system BC1. In this system initial half length of the wall is thermally insulated and then a magnet coil and then another half wall is heated uniformly. (a) Shows the case of 1-coil located at the center of the pipe for $\ell = 10d$. Case (b) is twice repeated of case (a) for $\ell = 20d$. Case (c) is three times repeated of case (a) for $\ell = 30d$.

Fig. 2 is the second system BC2. For a long pipe, the average temperature increases continuously which may

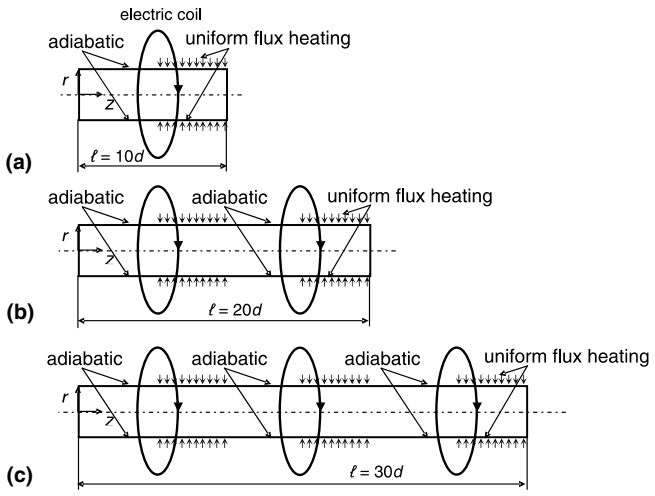

Fig. 1. Model system of BC1: (a) 1-coil for magnetic induction for $\ell = 10d$, (b) 2-coils for $\ell = 20d$ and (c) 3-coils for $\ell = 30d$.

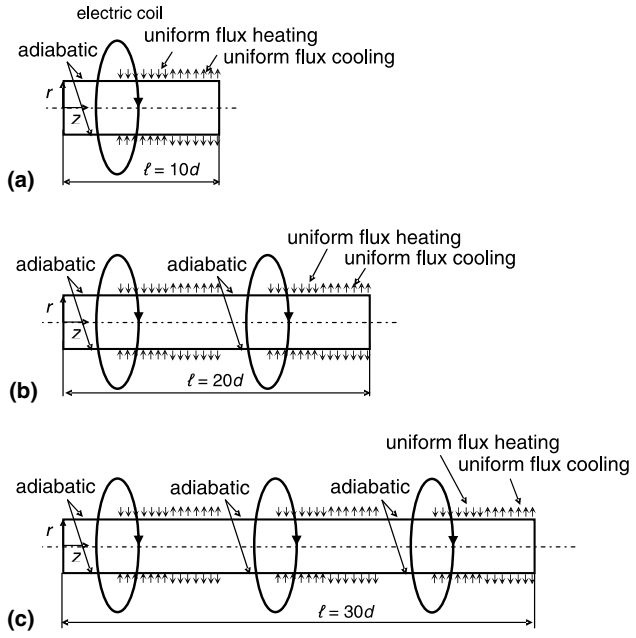

Fig. 2. Model system of BC2: (a) 1-coil for magnetic induction for $\ell = 10d$, (b) 2-coils for $\ell = 20d$ and (c) 3-coils for $\ell = 30d$.

not be preferable in the practical application. Thus we consider the case with cooling as BC2. In this system in case (a) the initial one-third of the pipe is an adiabatic wall, and a coil and next one-third wall has uniform flux heating and the final one-third wall is uniformly cooled. Case (b) is twice repeated of case (a) for $\ell = 20d$. Case (c) is three times repeated of case (a) for $\ell = 30d$.

Fig. 3(a) shows typical distributions of magnetic induction vector B for the case of 1-coil. Fig. 3(b) shows contour map of Bz, and Fig. 3(c) the vector of ∇B^2 which is proportional to the magnetic force.

Air is used as a representative paramagnetic fluid in this report. The basic hydrodynamic assumptions for the model include the fluid being Newtonian and incompressible, the

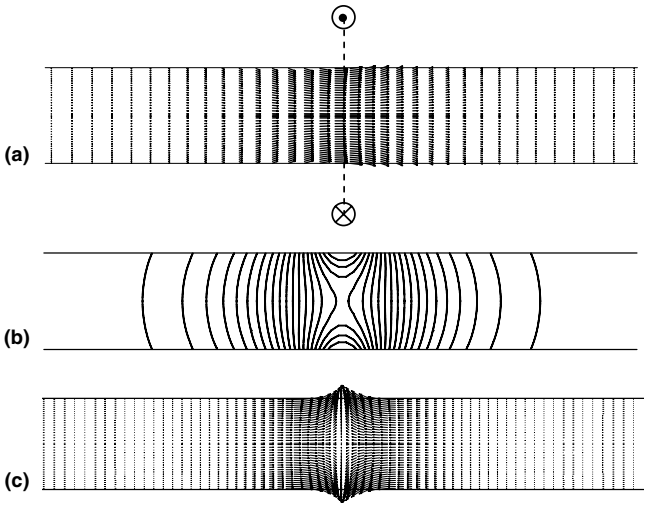

Fig. 3. Typical distributions of magnetic field induction: (a) vector of $\vec{B}$, (b) contour map of Bz and (c) vector of ∇B^2.

flow being laminar and viscous dissipation being negligible, the thermodynamic property of fluid being constant except magnetic susceptibility and density, natural convection caused by gravitational buoyancy force being negligible for a space condition. The 2-D continuity and momentum equations including the magnetic force term and energy equation in cylindrical coordinate (R, Z) according to Tagawa et al. [6]:

Equation of continuity:

$$\frac{1}{R}\frac{\partial}{\partial R}(RU) + \frac{\partial W}{\partial Z} = 0 \tag{2}$$

Momentum equations:

R-Direction:

$$\frac{\partial U}{\partial \tau} + U\frac{\partial U}{\partial R} + W\frac{\partial U}{\partial Z} = -\frac{\partial P}{\partial R} + \left[\frac{\partial}{\partial R}\left(\frac{1}{R}\frac{\partial}{\partial R}(RU)\right) + \frac{\partial^2 U}{\partial Z^2}\right] - \xi\Theta\frac{\partial B^2}{\partial R} \tag{3a}$$

Z-Direction:

$$\frac{\partial W}{\partial \tau} + U\frac{\partial W}{\partial R} + W\frac{\partial W}{\partial Z} = -\frac{\partial P}{\partial Z} + \left[\frac{1}{R}\frac{\partial}{\partial R}\left(R\frac{\partial W}{\partial R}\right) + \frac{\partial^2 W}{\partial Z^2}\right] - \xi\Theta\frac{\partial B^2}{\partial Z} \tag{3b}$$

Energy equation:

$$\frac{\partial \Theta}{\partial \tau} + U\frac{\partial \Theta}{\partial R} + W\frac{\partial \Theta}{\partial Z} = \frac{1}{Pr}\cdot\left(\frac{1}{R}\frac{\partial}{\partial R}\left(R\frac{\partial \Theta}{\partial R}\right) + \frac{\partial^2 \Theta}{\partial Z^2}\right) \tag{4}$$

Magnetic induction is computed from Biot–Savart's law:

$$\vec{B} = -\frac{1}{4\pi}\oint\frac{\vec{R}\times d\vec{S}}{R^3} \tag{5}$$

Dimensionless variables employed in the above equations are as follows:

$$R=\frac{r}{d};\quad Z=\frac{z}{d};\quad L=\frac{l}{d};\quad S=\frac{s}{d};\quad U=\frac{u}{v_0/d}$$
$$W=\frac{w}{v_0/d};\quad \tau=\frac{t}{d^2/v_0};\quad P=\frac{p}{\rho_0 v_0^2/d^2}$$
$$\Theta=\frac{T-T_{\text{in}}}{T_{\text{ref}}};\quad Pr=\frac{v_0}{\alpha_0}$$
$$T_{\text{ref}}=(-q_{\text{w}}d)/\lambda_0\quad\text{for heating}$$
$$T_{\text{ref}}=(q_{\text{w}}d)/\lambda_0\quad\text{for cooling}\qquad(6)$$
$$B=\frac{b}{b_0};\quad b_0=\mu_{\text{m}}i/d$$
$$\xi=\frac{\chi_{\text{m}0}b_0^2}{\mu_{\text{m}}}\frac{\beta_0 d^2 T_{\text{ref}}}{v_0^2}$$

where ξ is a combination of diameter d, equivalent temperature T_{ref}, and reference magnetic induction b_0 to represent the strength of the magnetic field. Other reference properties are at the reference temperature.

The initial condition is

$$U=W=0,\quad \Theta=0\qquad(7)$$

Boundary conditions are

at an inlet:

$$P=P_{\text{in}}=0;\quad \frac{\partial U}{\partial Z}=0;\quad \Theta=0$$

at an outlet:

$$P=P_{\text{ou}}=0;\quad \frac{\partial U}{\partial Z}=0;\quad \frac{\partial \Theta}{\partial Z}=0$$

for BC1 at $R=0.5$:

$$U=W=0$$
$$\frac{\partial\Theta}{\partial R}=0\quad\text{at}\quad\left(\frac{j-1}{n}\cdot L\right)\leqslant Z<\left(\frac{2j-1}{2n}\cdot L\right)$$
$$\frac{\partial\Theta}{\partial R}=1\quad\text{at}\quad\left(\frac{2j-1}{2n}\cdot L\right)\leqslant Z<\left(\frac{j}{n}\cdot L\right)$$

for BC2 at $R=0.5$:

$$U=W=0$$
$$\frac{\partial\Theta}{\partial R}=0\quad\text{at}\quad\left(\frac{j-1}{n}\cdot L\right)\leqslant Z<\left(\frac{3j-2}{3n}\cdot L\right)$$
$$\frac{\partial\Theta}{\partial R}=1\quad\text{at}\quad\left(\frac{3j-2}{3n}\cdot L\right)\leqslant Z<\left(\frac{3j-1}{3n}\cdot L\right)\qquad(8)$$
$$\frac{\partial\Theta}{\partial R}=-1\quad\text{at}\quad\left(\frac{3j-1}{3n}\cdot L\right)\leqslant Z<\left(\frac{j}{n}\cdot L\right)$$

where n is a total number of coils and j takes integer from 1 to n.

Static pressure boundary condition [7] is employed at the inlet and the outlet since the flow rate may not be constant with an application of various magnetic fields. The similar pressure boundary conditions were successfully employed by Lee et al. [8] for the effect of magnetic field on human breathing.

3. Numerical methods

The finite-volume technique based on the SIMPLE [9] and SIMPLEC [10] pressure–velocity coupling algorithm, with non-uniform staggered grid system, is used to solve the transient two-dimensional model Eqs. (2)–(4). Diffusion terms are approximated by the central difference scheme and convection terms by QUICK scheme [11]. At each step, SIMPLE algorithm with pressure boundary condition for momentum equations and SIMPLEC algorithm for other equations are iterated until the mass, momentum and enthalpy residuals converge less than 10^{-4}.

The grid number dependence is tested and listed in Table 1. For $Re_0=100$, the relative difference is about 0.107% for 32×302, at $L=10$. Thus following grid numbers are employed, i.e., 32×302 for $L=10$, 62×602 for $L=20$ and 92×902 for $L=30$, respectively.

4. Results and discussion

4.1. Effect of pipe length and number of coils on the flow rate

Pressure drop increases with the pipe length. In our previous report [4] with a single coil, the magnetic field was more effective on shorter channel than longer channel. The effect was less for larger diameter pipe than for smaller one.

Fig. 4 shows the resulted volume flow rate Re versus the magnetic strength ξ: (a) is for BC1 and (b) is for BC2. The parameter is a number of electric-coils, i.e., 1-coil for $L=10$, 2-coils for $L=20$ and 3-coils for $L=30$. The flow rates increase with the magnetic field for all cases. Furthermore the enhancement of flow rate are approximately similar, although flow rates for $L=20$ with 2-coils and $L=30$ with 3-coils are slightly smaller than that $L=10$ with 1-coil. This suggests that the multiple magnetic fields are effective to drive the fluid equally even for a longer pipe to overcome the viscous shear stress. There appears to be no more difference in the bulk flow rate Re between the

Table 1
Effect of grid numbers on the average Reynolds number for the fully developed laminar air flow without magnetic field and heat transfer, at $L=10$ and theoretical $Re=100$

Grids in $R\times Z$ coordinate	Computed Reynolds number	Relative error (%)
12×102	100.892	0.892
22×102	100.220	0.220
22×202	100.220	0.220
32×102	100.104	0.104
32×202	100.101	0.101
32×302	100.107	0.107
42×102	100.066	0.066
42×202	100.063	0.063
42×302	100.067	0.067
42×402	100.076	0.076

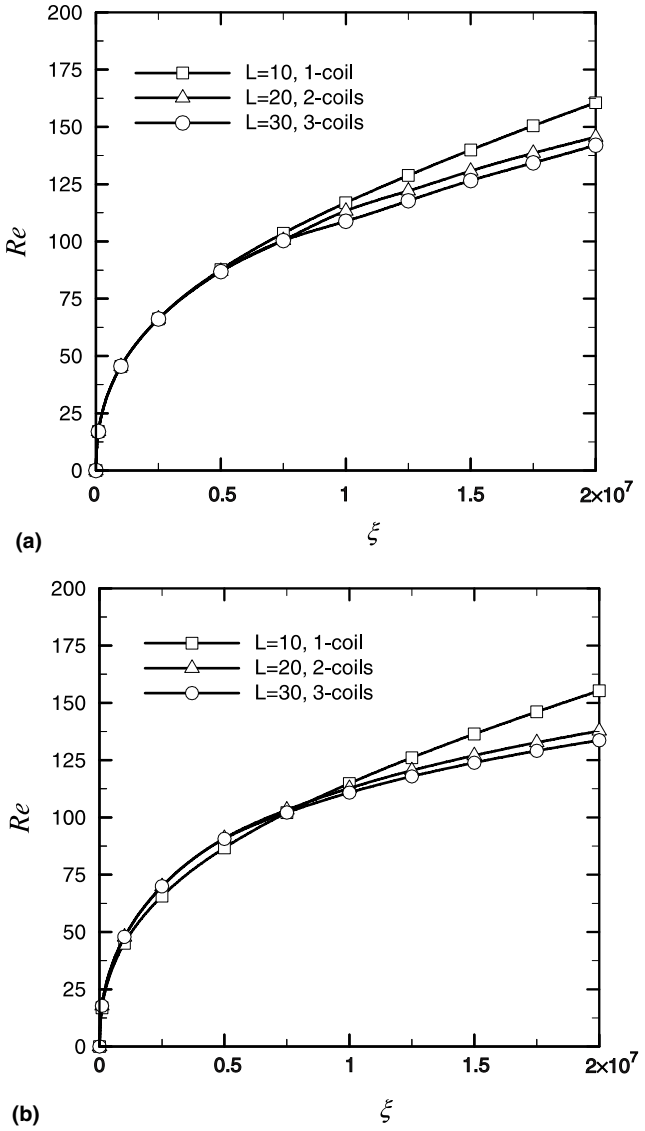

Fig. 4. Effect of ξ and coil numbers on the flow rate Re for three axial dimensionless lengths, $L = 10$ with 1-coil, $L = 20$ with 2-coils and $L = 30$ with 3-coils: (a) BC1 and (b) BC2.

system BC1 and BC2, although BC2 has the cooling operation from the wall. Followings are more detailed pressure and temperature characteristics.

4.2. Distribution of cross-sectional magnetic force

Fig. 5 shows the distributions of cross-sectional magnetic force, F_{mz}, along the axial direction for $\xi = 10^7$ for three cases. Fig. 5(a) shows those for BC1. Fig. 5(b) shows the enlarged figure of (a) at the first coil. From the definition of the magnetic force F_{mz} and dimensionless temperature Θ, the value of magnetic force is zero at the first half length, since the dimensionless temperature is equal zero at the inlet. Fig. 5(b) shows that the distribution of magnetic force at the first coil is almost similar for three cases. In Fig. 5(a), at the second and third coils, the magnetic force is negative before the coils to suggest that the heated fluid is repelled by

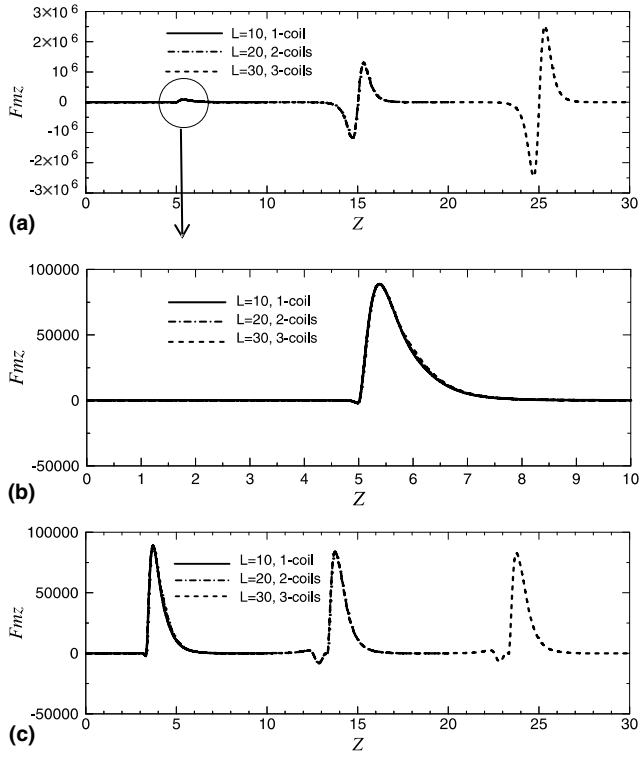

Fig. 5. Comparison with distribution of cross-sectional magnetic force, F_{mz}, along the axial direction for 1-coil for $L = 10$, 2-coils for $L = 20$, and 3-coils for $L = 30$, at $\xi = 10^7$: (a) BC1, (b) enlarged figure of (a) at the first coil and (c) BC2.

a strong magnetic force since the present fluid is paramagnetic fluid. However, total pressure gradient initially given for fluid overcomes this repelling force to pass through the magnetic field. Then the fluid is repelled downstream due to the higher temperature (larger magnetic force).

The magnitude and the shapes of magnetic force differ seriously between Fig. 5(a) BC1 and (c) BC2. The reason for this is because at BC1 the temperature of air is increased at the first coil and air receives repelling effect at the second and third coils. The air is driven more strongly downward due to the higher temperature than that at the first coil since magnetic force is proportional to the temperature as seen in the last term of Eqs. (3). On the other hand, for BC2 the magnetic forces along the pipe for the second and third coils are at almost similar magnitude as the first coil because the fluid is cooled from the wall and the fluid temperature becomes similar to the inlet fluid one and similar strength of magnetic force. The magnitudes of the ordinate are the same scale as Fig. 5(b) and (c). This means the magnetic force for BC2 is just the same magnitude for the first coil in Fig. 5(a). However, the total effect for the flowing rate is similar for BC1 and BC2 as shown in Fig. 4.

4.3. Distribution of pressure and pressure gradient

Fig. 6 shows the pressure along the axial direction for $\xi = 10^7$. Fig. 6(a) is for BC1, Fig. 6(b) an enlarged figure

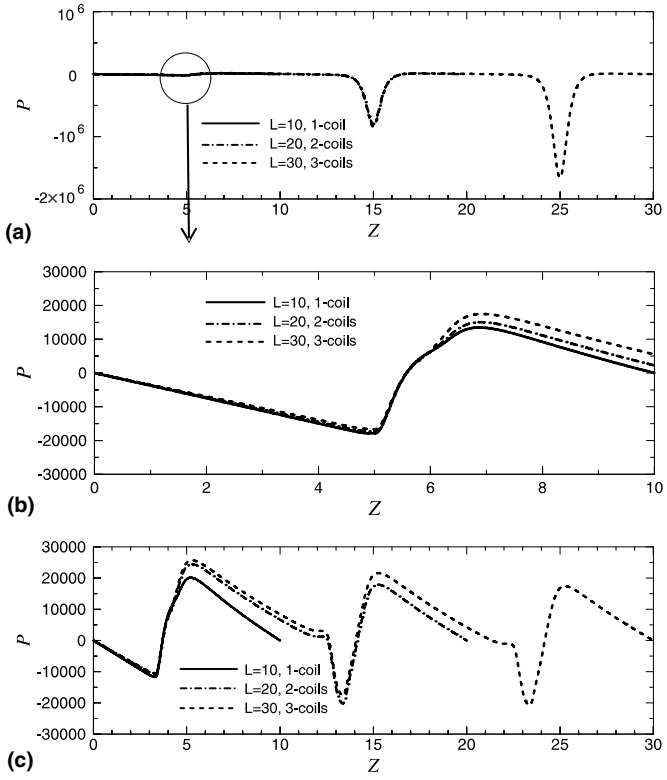

Fig. 6. Comparison with distribution of pressure, P, along the axial direction for 1-coil for $L = 10$, 2-coils for $L = 20$, and 3-coils for $L = 30$, at $\xi = 10^7$: (a) BC1, (b) enlarged figure of (a) at the first coil and (c) BC2.

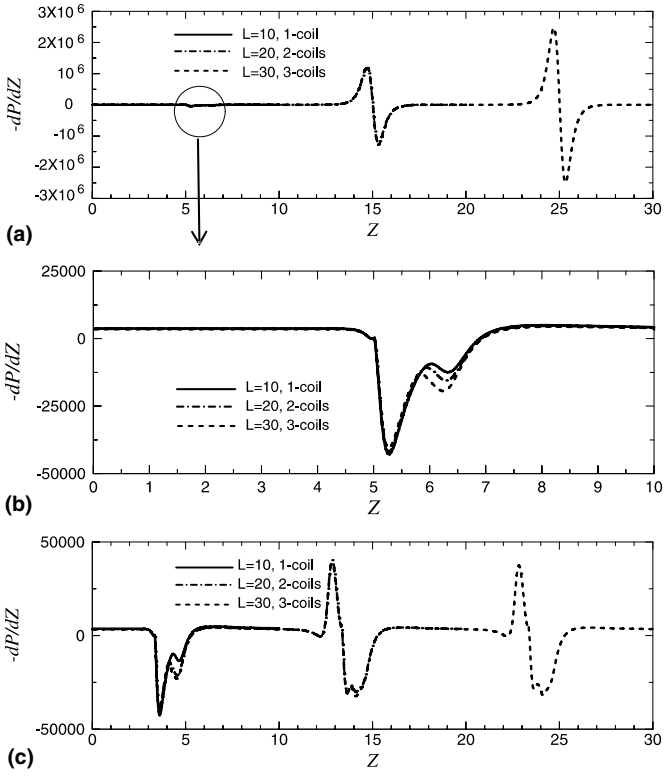

Fig. 7. Comparison with distribution of pressure gradient, $-\mathrm{d}P/\mathrm{d}Z$, along the axial direction for 1-coil for $L = 10$, 2-coils for $L = 20$, and 3-coils for $L = 30$, at $\xi = 10^7$: (a) BC1, (b) enlarged figure of (a) at the first coil and (c) BC2.

at the first coil and Fig. 6(c) for BC2. Without a magnetic field pressure is uniform. Right after the application of magnetic field as seen in (b), the magnetic force acts and increases the pressure at Z greater than 5, the location of first coil. Although at the beginning there is no pressure difference between the inlet and outlet, pressure redistributes along the axial direction when the magnetic force works. The effective length of the magnetic force can be revealed from the pressure profiles. Fig. 6(c) shows pressure distribution for system BC2 with cooling from the wall. Three cases are almost similar each other in the first section and the subsequent sections are almost alike due to the similar temperature as the previous sections by cooling. However, the pressure profiles do not return to the inlet value at $Z = 10$ and 20 for 2- and 3-coils cases.

Fig. 7 shows negative pressure gradient to accompany with Fig. 6. Pressure gradient represents the force per volume and may be more understandable to follow the effect of the magnetic force. As shown in (b) enlarged figure of (a) at the first coil, negative pressure gradient decreases extensively after a coil to drive the flow in the downstream of the main flow. The pressure gradient fluctuates but returns to the original value where the magnetic field is no more effective. In (c) for BC2, there are upward peak in negative pressure gradient just in front of the second and third coils in contrast to the first one. These would be because the flow does not come back to the original states as seen in Fig. 6(c).

4.4. Distribution of cross-sectional temperature

Converged distributions of cross-sectional average temperature along the axial direction are shown in Fig. 8 for 1-coil for $L = 10$, 2-coils for $L = 20$, and 3-coils for $L = 30$, at $\xi = 10^7$. Fig. 8(a) is for BC1 and Fig. 8(b) for BC2. For BC1 the cross-sectional temperatures increase

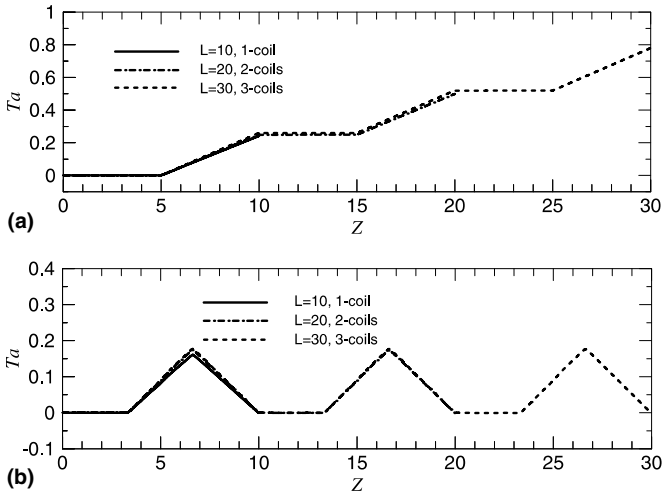

Fig. 8. Distribution of cross-sectional average temperature along the axial direction for 1-coil for $L = 10$, 2-coils for $L = 20$, and 3-coils for $L = 30$, at $\xi = 10^7$: (a) BC1 and (b) BC2.

with the increase of the pipe lengths for all three cases, as in this system the pipe walls are only heated. For BC2 the cross-sectional temperatures increase and decrease periodically along the axial direction for all three pipe lengths, as in this system the pipe wall is adiabatic in the initial one-third of wall, uniform flux heating for the next one-third length and uniform heat flux cooling for the final one-third length. These results show the temperature distribution are almost equivalent for three lengths.

5. Conclusions

Fully transient two-dimensional model equations with static pressure boundary condition are numerically solved for the laminar air flow under a magnetic field in a circular pipe. The converged axial pressure and pressure gradient distribution reveal the effect of magnetic force as an additional source of driving force to enhance the volume flow rate. The acting region depends on the combination of strength of magnetic field and temperature difference distributions.

For the same ξ the flow rates decrease for a longer pipe due to viscous shear stress on the wall. For the system with cooling, the flow characteristics are similar, but the fluid temperature does not increase continuously. The present computation may suggest magnetic force of multiple coils and cooling may work as driving pumps for air flow in a long pipe.

Acknowledgements

This work was partly supported by the visiting researcher fund of the Key Laboratory of Enhanced Heat Transfer and Energy Conservation, Ministry of Education, China.

References

[1] H. Uetake, J. Nakagawa, N. Hirota, K. Kitazawa, Nonmechanical magnetothermal wind blower by a superconducting magnet, J. Appl. Phys. 85 (1999) 5735–5737.
[2] H. Uetake, N. Hirota, J. Nakagawa, Y. Ikezoe, K. Kitazawa, Thermal convection control by gradient magnetic field, J. Appl. Phys. 87 (2000) 6310–6312.
[3] S.S. Lu, C.H. Lee, T. Tagawa, H. Ozoe, B. Hua, Enhancement of heat transfer and flow rates of air flow in a pipe with an application of a magnetic field, J. Enhanc. Heat Transfer 10 (2003) 45–60.
[4] S.S. Lu, C.H. Lee, T. Tagawa, H. Ozoe, B. Hua, Magnetically controlled air flow and heat transfer in a pipe with uniform wall heat flux on its latter half length, Numer. Heat Transfer A 45 (2004) 377–390.
[5] B. Bai, A. Yabe, J. Qi, N.I. Wakayama, Quantitative analysis of air convection caused by magnetic-fluid coupling, AIAA J. 37 (1999) 1538–1543.
[6] T. Tagawa, R. Shigemitsu, H. Ozoe, Magnetizing force modeled and numerically solved for natural convection of air in a cubic enclosure: effect of the direction of the magnetic field, Int. J. Heat Mass Transfer 45 (2002) 267–277.
[7] K.M. Kelkar, D. Choudhury, Numerical method for the prediction of incompressible flow and heat transfer in domains with specified pressure boundary conditions, Numer. Heat Transfer B 38 (2000) 15–36.
[8] C.H. Lee, S.S. Lu, T. Tagawa, H. Ozoe, J.M. Hyun, Numerical analysis of magnetic effect on human breathing, JSME Int. J. Series C 46 (2003) 572–582.
[9] S.V. Patankar, Numerical Heat Transfer and Fluid Flow, Hemisphere, New York, 1980, p. 126.
[10] J.R. van Doormal, G.D. Raithby, Enhancements of the SIMPLE method for predicting incompressible flows, Numer. Heat Transfer 7 (1984) 147–163.
[11] T. Hayase, J.A.C. Humphrey, R. Greif, A consistently formulated QUICK scheme for fast and stable convergence using finite-volume iterative calculation procedures, J. Comput. Phys. 98 (1992) 108–118.